

# Measuring black hole spin through gravitational lensing of pulsars

Amjad Ashoorioon\* and Mohammad Bagher Jahani Poshteh†

*School of Physics, Institute for Research in Fundamental Sciences (IPM), P.O. Box 19395-5531, Tehran, Iran*

Robert B. Mann‡

*Department of Physics and Astronomy, University of Waterloo, Waterloo, Ontario, N2L 3G1, Canada and  
Perimeter Institute for Theoretical Physics, Waterloo, Ontario, N2L 2Y5, Canada*

We put forward a new procedure for measuring the spin of a black hole with unprecedented accuracy based on gravitational lensing of millisecond pulsars. The deflection angle of light increases by increasing the rotation parameter. For primary and secondary images the angular positions are larger for rotating black holes by an amount of the order of microarcseconds. Also, the differential time delay for the case of a rotating black hole is larger than that for the non-rotating case and the difference could be as large as a few seconds. We show that this quantity could help us achieve an extremely precise measurement of the black hole spin, much more accurate than the current and near future achievable estimation of black hole spin through other methods.

The spin of a black hole is an important property that can reveal information about its origin, evolution, and environment. For supermassive black holes, knowledge their spin could help us test and constrain different formation scenarios, such as gas cloud collapse, mergers from smaller black holes, or accretion of surrounding matter [1]. The spin also affects the energy output, radiation efficiency, gravitational wave emission, and space-time distortion of the black hole, which have important implications for feedback processes, observability, and tests of general relativity [2–4]. Measurement of black hole spin is therefore a crucial task for understanding these fascinating objects and their role in cosmic history.

Many methods have been developed or applied to estimate the spins of black holes. In the Fe-K $\alpha$  method one observes the X-ray emission from the iron atoms in the accretion disk, which is distorted by the strong gravity and rotation of its accompanying black hole [5–7]. Another method is X-ray polarimetry, which is based on observing the polarization properties of the X-ray radiation emitted by the accretion disk, because the polarization of X-ray photons is affected by the strong gravity and rotation of the black hole [8–10]. Other methods include using the shape and size of the black hole shadow [11–13], gravitational wave observations [14], the observed transition of the jet boundary shape [15], observed twisted light propagating near a rotating black hole [16], and modelling the jet power and the accretion rate [17, 18].

In this Letter, working in the context of general relativity, we propose a new method for measuring the spin of black holes with extraordinary accuracy. Our method is based on the gravitational lensing of millisecond (or mildly-recycled [19]) pulsars with periods  $P \lesssim 30\text{ms}$  ( $20\text{ms} \lesssim P \lesssim 100\text{ms}$ ). Millisecond pulsars are very important for astrophysics and cosmology as they can be

used as precise clocks to measure various phenomena in the universe. Recently, by observing the tiny changes in the arrival times of the radio pulses from these pulsars, the NANOGrav collaboration has found compelling evidence that pulsar timing is affected by the gravitational wave background, opening a new window for exploring gravitational wave emission [20].

There have been several attempts to study gravitational lensing by spinning black holes [21–29]. Most of them work in either the strong or weak field limits, in which the deflection angle is expanded near the photon circle or near infinity, respectively. However in a gravitational lensing event, the light trajectory starts from a source that is usually taken to be at a distance far from the black hole (lens), reaches a turning point near the black hole, and then escapes to the observer, who is also far from the black hole. The light ray therefore experiences both the weak and strong field regimes along its single trajectory, and neither weak nor strong field approximations alone can describe the event accurately. (Another criticism against the strong field approximation has been raised in [30].)

Here we generalize the numerical methods of [31–33] for rotating black holes to study gravitational lensing by Kerr black holes. In this method, we numerically solve the lens equation to find the distance of the closest approach (to the black hole) and other lensing quantities. We note that we only consider light rays on the equatorial plane of a rotating black hole. We use units in which  $G = c = 1$  and metric signature  $+2$ .

The scenario we study is presented in Fig. 1. The ray of light that is coming from the source S (which we assume to be a pulsar) is deflected by the black hole. The observer cannot see the source in its actual place but sees its lensed images. One image is on the same side of the black hole as the source. This image is called the primary image. Another image is on the opposite side of the black hole and is called the secondary image.

The metric of a Kerr spacetime is

$$ds^2 = g_{tt}dt^2 + g_{t\phi}dtd\phi + g_{r\phi}dr^2 + g_{\theta\theta}d\theta^2 + g_{\phi\phi}d\phi^2, \quad (1)$$

\* amjad@ipm.ir

† jahani@ipm.ir

‡ rbmann@uwaterloo.ca

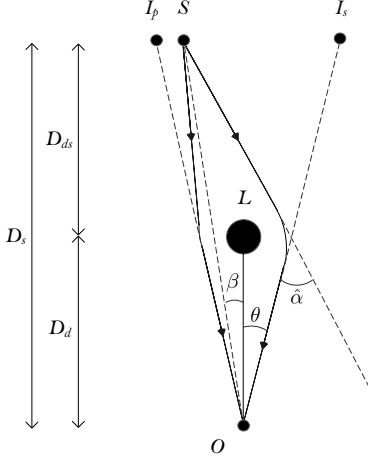


FIG. 1. The lens diagram. The light ray which is coming from the source  $S$  (which we take to be a pulsar) would be deflected near the black hole (lens)  $L$ . The observer  $O$  would see images of the source, one on the same side as the source (with respect to the line of sight to  $L$ ), which is called the primary image  $I_p$ , and another one on the opposite side of the source, which is called the secondary image  $I_s$ .

where

$$g_{tt} = -\left(1 - \frac{2mr}{\Sigma}\right), \quad (2)$$

$$g_{t\phi} = \frac{4mar \sin^2 \theta}{\Sigma}, \quad (3)$$

$$g_{rr} = \frac{r^2 - 2mr + a^2}{r^2 - 2mr + a^2}, \quad (4)$$

$$g_{\theta\theta} = \Sigma, \quad (5)$$

$$g_{\phi\phi} = \left(r^2 + a^2 + \frac{2ma^2r \sin^2 \theta}{\Sigma}\right) \sin^2 \theta, \quad (6)$$

and

$$\Sigma \equiv r^2 + a^2 \cos^2 \theta. \quad (7)$$

In these relations  $m$  is the mass of Kerr black hole and  $a$  is its rotation parameter.

The geodesics are found by using the Lagrangian

$$\mathcal{L} = \frac{1}{2} g_{\mu\nu} \dot{x}^\mu \dot{x}^\nu, \quad (8)$$

where the dot shows differentiation with respect to some affine parameter. The constants of motion are

$$E = -\frac{\partial \mathcal{L}}{\partial \dot{t}} = -\frac{1}{2} (2g_{tt} \dot{t} + g_{t\phi} \dot{\phi}), \quad (9)$$

$$L_z = -\frac{\partial \mathcal{L}}{\partial \dot{\phi}} = -\frac{1}{2} (g_{t\phi} \dot{t} + 2g_{\phi\phi} \dot{\phi}). \quad (10)$$

Consider null geodesics on the equatorial plane of the black hole, for which  $\theta = \frac{\pi}{2}$  and  $\dot{\theta} = 0$  and  $\mathcal{L} = 0$ . Hence from Eq. (8) we have

$$g_{tt} \dot{t}^2 + g_{t\phi} \dot{t} \dot{\phi} + g_{rr} \dot{r}^2 + g_{\phi\phi} \dot{\phi}^2 = 0, \quad (11)$$

which results in

$$\frac{g_{tt} \dot{t}^2 + g_{t\phi} \dot{t} \dot{\phi}}{g_{\phi\phi} \dot{\phi}^2} + \frac{g_{rr}}{g_{\phi\phi}} \left(\frac{dr}{d\phi}\right)^2 = -1. \quad (12)$$

Substituting for  $\dot{t}$  and  $\dot{\phi}$  from Eqs. (9) and (10) yields

$$\frac{(2g_{\phi\phi} E - g_{t\phi} L_z) (2g_{\phi\phi} g_{tt} E + g_{t\phi} g_{tt} L_z - g_{t\phi}^2 E)}{g_{\phi\phi} (g_{t\phi} E - 2g_{tt} L_z)^2} + \frac{g_{rr}}{g_{\phi\phi}} \left(\frac{dr}{d\phi}\right)^2 = -1. \quad (13)$$

At the point of closest approach,  $r = b$ , we have  $dr = 0$ , so

$$\frac{2g_{\phi\phi}(b)E - g_{t\phi}(b)L_z}{g_{\phi\phi}(b) [g_{t\phi}(b)E - 2g_{tt}(b)L_z]^2} \times [2g_{\phi\phi}(b)g_{tt}(b)E + g_{t\phi}(b)g_{tt}(b)L_z - g_{t\phi}^2(b)E] = -1. \quad (14)$$

Eq. (14) can be solved for the ratio  $\eta = \frac{L_z}{E}$  as a function of  $b$ , yielding

$$\eta = \frac{g_{t\phi}(b) - \sqrt{g_{t\phi}^2(b) - 4g_{\phi\phi}(b)g_{tt}(b)}}{2g_{tt}(b)}. \quad (15)$$

for the impact parameter  $\eta$ , with the sign chosen so that the static case is recovered as  $a \rightarrow 0$  [31–33].

By using the parameter  $\eta$  one can rewrite Eq. (13) as

$$\frac{d\phi}{dr} = \sqrt{\frac{g_{rr}}{g_{\phi\phi}}} \times \left[ -1 - \frac{(2g_{\phi\phi} - g_{t\phi}\eta) (2g_{\phi\phi}g_{tt} + g_{t\phi}g_{tt}\eta - g_{t\phi}^2)}{g_{\phi\phi} (g_{t\phi} - 2g_{tt}\eta)^2} \right]^{-1/2} \equiv \Gamma. \quad (16)$$

The deflection angle is then

$$\hat{\alpha}(b) = 2 \int_b^\infty \Gamma dr - \pi. \quad (17)$$

Eq. (11) can also be written as

$$\frac{(2g_{tt}L_z - g_{t\phi}E) (2g_{\phi\phi}g_{tt}L_z + g_{\phi\phi}g_{t\phi}E - g_{t\phi}^2L_z)}{g_{tt} (g_{t\phi}L_z - 2g_{\phi\phi}E)^2} + \frac{g_{rr}}{g_{tt}} \left(\frac{dr}{dt}\right)^2 = -1. \quad (18)$$

At  $r = b$  we have  $dr = 0$ . This can be used to find the same  $\eta$  as in Eq. (15). Therefore from Eq. (18) we obtain

$$\frac{dt}{dr} = \sqrt{\frac{g_{rr}}{g_{tt}}} \times \left[ -1 - \frac{(2g_{tt}\eta - g_{t\phi}) (2g_{\phi\phi}g_{tt}\eta + g_{\phi\phi}g_{t\phi} - g_{t\phi}^2\eta)}{g_{tt} (g_{t\phi}\eta - 2g_{\phi\phi})^2} \right]^{-1/2} \equiv \Pi \quad (19)$$

from which we compute the time delay

$$\tau(b) = \int_b^{r_s} \Pi dr + \int_b^{D_d} \Pi dr - D_s \sec \beta, \quad (20)$$

where  $D_s = D_d + D_{ds}$  and  $r_s = \sqrt{D_{ds}^2 + D_s^2 \tan^2 \beta}$ . Defined in this way, the time delay is the difference between the time it takes light to travel from source to observer in the physical spacetime (with the black hole), and the time it would take to travel from source to observer in flat spacetime (with no black hole).

Using the geometrical arguments we can write

$$\eta = D_d \sin \theta. \quad (21)$$

and in turn obtain the Virbhadra-Ellis lens equation [31]

$$\tan \beta = \pm \{ \tan \theta - \mathcal{D} [\tan \theta + \tan(\hat{\alpha} - \theta)] \}, \quad (22)$$

where  $\mathcal{D} = D_{ds}/D_s$ . The plus/minus signs correspond to primary/secondary images and

$$\mu = \left( \frac{\sin \beta}{\sin \theta} \frac{d\beta}{d\theta} \right)^{-1} \quad (23)$$

is the image magnification. To find  $\frac{d\beta}{d\theta}$  we use the lens equation (22), which implies computing  $\frac{d\hat{\alpha}}{d\theta} = \frac{d\hat{\alpha}}{db} \frac{db}{d\theta}$ . The second factor can be obtained from (15) and (21). We calculate the first factor numerically.

Now we investigate the primary and secondary images produced in gravitational lensing by a rotating black hole and compare these to the non-rotating case of the same mass. Specifically, we consider the black hole at the center of the M87 galaxy, with mass  $M_{M87^*} = 9.6 \times 10^{12} m \equiv 6.5 \times 10^9 M_\odot$  and distance  $D_d = 5.2 \times 10^{23} m \equiv 16.8$  Mpc [34].

In Tables I and II we present the image positions, deflection angles, magnification, and (differential) time delay of primary and secondary images for different values of angular source positions. For illustrative purposes, we have taken the black hole to be halfway between the source and the observer. Although no pulsars have yet been observed at this distance, pulsars have been observed at distances comparable to that of M87 [35], and it is conceivable that future observations will detect pulsars even further away. Note that the image angle is relative to the lens-observer axis in Fig. 1 and is always positive.

From Table I we see that the deflection angle is larger for rotating black holes. We also see that the angular positions of primary and secondary images are larger if the black hole is rotating; for the values considered in this table and for small values of angular source position, the difference can be as large as a few microarcseconds. The difference between the rotating and non-rotating cases for the angular position of the primary image decreases by with increasing angular source position. On the other hand, the corresponding value for secondary image increases by increasing  $\beta$ .

From Table II we see that for primary images the magnification is larger if the black hole is non-rotating. The difference between the primary image magnification in the rotating and non-rotating cases,  $\mu_{p,a^*=0.99} - \mu_{p,a^*=0}$ , is a negative quantity and its absolute value decreases with increasing angular position of the source. Furthermore, the absolute value of the magnification of secondary images is larger if the lens is non-rotating. Since the magnification of secondary images is defined to be negative, the quantity  $\mu_{s,a^*=0.99} - \mu_{s,a^*=0}$  is positive, and its value decreases with increasing  $\beta$ .

In Table II we also see that the time delay of primary images decreases by increasing the source angular position for both rotating and non-rotating cases. This quantity is larger if the lens is a rotating black hole. We have presented the time delay of secondary images. Instead we have shown the differential time delay  $t_d = \tau_s - \tau_p$ . This quantity is of considerable observational importance: if the source is pulsating, every phase in its period appears in the secondary image  $t_d$  seconds after it has appeared in the primary image. This differential time delay increases with increasing angular position of the source. It is larger if the black hole is rotating; for the values chosen in Table II, and for large values of  $\beta$  the difference can be as large as a few seconds. The difference between the differential time delay in the case of rotating black hole and the case of non-rotating black hole,  $t_{d,a^*=0.99} - t_{d,a^*=0}$ , gets larger as  $\beta$  increases.

We have also studied the behavior of lensing parameters for a range of values of the rotation parameter (details will be presented elsewhere.) The angular positions of both primary and secondary images increases with increasing the rotation parameter, whereas the magnification of the primary image and the absolute value of the magnification of secondary image decreases. The differential time delay increases with increasing rotation parameter. Details of the behavior of lensing parameters as a function of  $\mathcal{D}$  will be presented in a forthcoming publication.

We do not see the source in its real place and therefore we cannot measure  $\beta$  directly. However, it is possible to find  $\beta$  from the angular positions of primary and secondary images. Suppose that we observe primary and secondary images; these can be distinguished from their magnifications. From Table II we see that the absolute value of the magnification of the primary image is larger than that of the secondary image for both the rotating and non-rotating cases. We can find the distance to the source by, for example, using the red shift of the images. Suppose also that we know the mass of the lens and our distance to it. What we do not know are  $\beta$  and if the lens is rotating or not. The primary image can be due to lensing by a rotating black hole and a source at position  $\beta_{p,ro}$  or due to lensing by a non-rotating black hole and a source at position  $\beta_{p,nr}$ . On the other hand, The secondary image can be due to a rotating black hole and a source at position  $\beta_{s,ro}$  or due to lensing by a non-rotating black hole and a source at position  $\beta_{s,nr}$ . We

TABLE I. Image positions  $\theta$  and deflection angles  $\hat{\alpha}$  of primary and secondary images due to lensing by rotating (ro) as well as non-rotating (nr) black holes.  $\beta$  is the angular source position and the subscripts  $p$  and  $s$  refer to primary and secondary images, respectively. All angles are in *arcseconds*. We have used  $m = M_{\text{M87}^*} = 9.6 \times 10^{12}$  m,  $D_d = 5.2 \times 10^{23}$  m and  $\mathcal{D} = 0.5$ . For the rotating black hole we have taken the rotation parameter to be  $a^* = 0.99$ .

$\beta$	Rotating black hole				Non-rotating black hole			
	$\theta_{p,\text{ro}}$	$\hat{\alpha}_{p,\text{ro}}$	$\theta_{s,\text{ro}}$	$\hat{\alpha}_{s,\text{ro}}$	$\theta_{p,\text{nr}}$	$\hat{\alpha}_{p,\text{nr}}$	$\theta_{s,\text{nr}}$	$\hat{\alpha}_{s,\text{nr}}$
0	1.2533650	2.5067300	1.2533650	2.5067300	1.2533631	2.5067262	1.2533631	2.5067262
0.1	1.3043613	2.4087225	1.2043614	2.6087229	1.3043594	2.4087188	1.2043595	2.6087190
0.5	1.5280523	2.0561047	1.0280571	3.0561143	1.5280508	2.0561017	1.0280549	3.0561098
1	1.8494124	1.6988249	0.8494216	3.6988431	1.8494113	1.6988225	0.8494190	3.6988379
2	2.6034054	1.2068108	0.6034216	5.2068432	2.6034047	1.2068094	0.6034185	5.2068371
3	3.4547138	0.9094276	0.4547318	6.9094636	3.4547134	0.9094267	0.4547285	6.9094569
4	4.3602762	0.7205524	0.3603017	8.7206034	4.3602759	0.7205519	0.3602982	8.7205964

TABLE II. Magnification  $\mu$  and (differential) time delay  $\tau$  ( $t_d = \tau_s - \tau_p$ ) of primary and secondary images due to lensing by rotating (ro) as well as non-rotating (nr) black holes.  $\beta$  and the subscripts  $p$  and  $s$  are as in Table I. (Differential) time delays are in *seconds*.  $m$ ,  $D_d$ ,  $\mathcal{D}$ , and  $a^*$  are as in Table I.

$\beta$	Rotating black hole				Non-rotating black hole			
	$\mu_{p,\text{ro}}$	$\tau_{p,\text{ro}}$	$\mu_{s,\text{ro}}$	$t_{d,\text{ro}}$	$\mu_{p,\text{nr}}$	$\tau_{p,\text{nr}}$	$\mu_{s,\text{nr}}$	$t_{d,\text{nr}}$
0	$\times$	1627269.6	$\times$	0	$\times$	1627269.3	$\times$	0
0.1	6.7850417	1617251.1	-5.7891987	20444.927	6.7850511	1617250.8	-5.7892080	20444.897
0.5	1.8260851	1580930.6	-0.8262814	102870.41	1.8260869	1580930.3	-0.8262832	102870.25
1	1.2669222	1542808.2	-0.2670980	209692.19	1.2669230	1542807.9	-0.2670988	209691.89
2	1.0565710	1484436.7	-0.0566955	448742.30	1.0565712	1484436.5	-0.0566958	448741.68
3	1.0176446	1441783.5	-0.0177282	737895.11	1.0176447	1441783.4	-0.0177284	737894.18
4	1.0068406	1408827.1	-0.0068980	1089190.1	1.0068407	1408827.0	-0.0068981	1089188.9

should note that for both primary and secondary images the source is the same source and the lens is the same black hole. Therefore, either  $\beta_{p,\text{ro}} = \beta_{s,\text{ro}}$  or  $\beta_{p,\text{nr}} = \beta_{s,\text{nr}}$  is true. This way it is possible to find  $\beta$  and determine if the black hole is rotating.

Most significantly, a measurement of differential time delay could help us find the rotation parameter with unprecedented precision. In fact, for large values of angular source position (of the order of arcseconds), a measurement of differential time delay with accuracy of  $\sim 10^{-4}$  seconds would result in a measurement of the spin parameter with less than 1 percent error. This is better than the most accurate estimates of M87\* spin that we can find, i.e. [16, 18], which are based on twisted light and accretion-jet analysis.

Recently it has been shown that LISA could constrain the spin to a precision as high as  $\Delta a^* \sim 10^{-10}$  [36]. Such a tight measurement is only possible for a near extremal black hole with spin parameter  $a^* = 1 - 10^{-9}$ . This value is far past the Thorne limit of  $a^* = 0.998$  [37]. For LISA to be able to constrain the spin, the black hole should constitute a binary system. Furthermore, the optimum mass to archive such precision is  $\sim 10^7 M_\odot$  [36], which is not a good method for M87\*, whose mass is  $\sim 10^9 M_\odot$ . By using the differential time-delay method we propose,

it is possible to find the spin with precision better than  $\Delta a^* \sim 10^{-10}$  if we could measure the differential time delay with accuracy  $10^{-11}$  seconds. Luckily, millisecond pulsars period can be measured with a very high precision — of the order of femtosecond [19, 38–40]. Therefore, if we have a pulsar as our source behind the black hole, a measurement of differential time delay with accuracy of the order  $10^{-11}$  seconds indeed seems feasible.

Our method can do better than LISA even for masses  $\sim 10^7 M_\odot$ . Consider for instance the supermassive black hole in M60-UCD1 galaxy with mass  $2.1 \times 10^7 M_\odot$  and distance 16.5 Mpc [41, 42]. To find its spin with precision better than  $\Delta a^* \sim 10^{-10}$  would require measuring the differential time delay with an accuracy of  $\sim 10^{-13}$  seconds. Unfortunately we have yet to observe any millisecond pulsars at such large distances. But we have several of them in our galactic neighborhood up to distances  $\sim 17.9$  kpc [43]. It is noteworthy that the method we have presented here can be used to measure the spins of lighter black holes that are present in our neighborhood. For example for the intermediate-mass black hole CO-0.40-0.22\* with mass  $\sim 10^5 M_\odot$  and distance 8.3 kpc a precision of  $\Delta a^* \sim 10^{-10}$  would be achieved if we measure the differential time delay with accuracy of  $\sim 10^{-15}$  seconds, within reach of present technology

[19, 38–40]. For stellar-mass black holes, however, a precision of  $\sim 10^{-19}$  seconds is needed.

*Acknowledgments:* This work was supported in part by

the Natural Sciences and Engineering Research Council of Canada.

- 
- [1] M. Volonteri, P. Madau, E. Quataert, and M. J. Rees, The Distribution and cosmic evolution of massive black hole spins, *Astrophys. J.* **620**, 69 (2005), arXiv:astro-ph/0410342.
- [2] R. D. Blandford and R. L. Znajek, Electromagnetic extractions of energy from Kerr black holes, *Mon. Not. Roy. Astron. Soc.* **179**, 433 (1977).
- [3] A. C. Fabian, Observational Evidence of AGN Feedback, *Ann. Rev. Astron. Astrophys.* **50**, 455 (2012), arXiv:1204.4114 [astro-ph.CO].
- [4] C. S. Reynolds, Observing black holes spin, *Nature Astron.* **3**, 41 (2019), arXiv:1903.11704 [astro-ph.HE].
- [5] A. C. Fabian, K. Iwasawa, C. S. Reynolds, and A. J. Young, Broad iron lines in active galactic nuclei, *Publ. Astron. Soc. Pac.* **112**, 1145 (2000), arXiv:astro-ph/0004366.
- [6] C. S. Reynolds and M. A. Nowak, Fluorescent iron lines as a probe of astrophysical black hole systems, *Phys. Rept.* **377**, 389 (2003), arXiv:astro-ph/0212065.
- [7] J. M. Miller, Relativistic X-ray Lines from the Inner Accretion Disks Around Black Holes, *Ann. Rev. Astron. Astrophys.* **45**, 441 (2007), arXiv:0705.0540 [astro-ph].
- [8] M. Dovciak, F. Muleri, R. W. Goosmann, V. Karas, and G. Matt, Thermal disc emission from a rotating black hole: X-ray polarization signatures, *Mon. Not. Roy. Astron. Soc.* **391**, 32 (2008), arXiv:0809.0418 [astro-ph].
- [9] L.-X. Li, R. Narayan, and J. E. McClintock, Inferring the Inclination of a Black Hole Accretion Disk from Observations of its Polarized Continuum Radiation, *Astrophys. J.* **691**, 847 (2009), arXiv:0809.0866 [astro-ph].
- [10] S. Schmoll, J. M. Miller, M. Volonteri, E. Cackett, C. S. Reynolds, A. C. Fabian, L. W. Brenneman, G. Miniutti, and L. C. Gallo, Constraining the Spin of the Black Hole in Fairall 9 with Suzaku, *Astrophys. J.* **703**, 2171 (2009), arXiv:0908.0013 [astro-ph.HE].
- [11] C. Bambi, K. Freese, S. Vagnozzi, and L. Visinelli, Testing the rotational nature of the supermassive object M87\* from the circularity and size of its first image, *Phys. Rev. D* **100**, 044057 (2019), arXiv:1904.12983 [gr-qc].
- [12] T. Kawashima, M. Kino, and K. Akiyama, Black Hole Spin Signature in the Black Hole Shadow of M87 in the Flaring State, *Astrophys. J.* **878**, 27 (2019), arXiv:1905.10717 [astro-ph.HE].
- [13] M. Afrin and S. G. Ghosh, EHT observables as a tool to estimate parameters of supermassive black holes, *Mon. Not. Roy. Astron. Soc.* **524**, 3683 (2023), arXiv:2307.08451 [gr-qc].
- [14] S. Vitale, R. Lynch, J. Veitch, V. Raymond, and R. Sturani, Measuring the spin of black holes in binary systems using gravitational waves, *Phys. Rev. Lett.* **112**, 251101 (2014), arXiv:1403.0129 [gr-qc].
- [15] E. E. Nokhrina, L. I. Gurvits, V. S. Beskin, M. Nakamura, K. Asada, and K. Hada, M87 black hole mass and spin estimate through the position of the jet boundary shape break, *Mon. Not. Roy. Astron. Soc.* **489**, 1197 (2019), arXiv:1904.05665 [astro-ph.HE].
- [16] F. Tamburini, B. Thidé, and M. Della Valle, Measurement of the spin of the M87 black hole from its observed twisted light, *Mon. Not. Roy. Astron. Soc.* **492**, L22 (2020), arXiv:1904.07923 [astro-ph.HE].
- [17] R. Nemmen, The Spin of M87\*, *Astrophys. J. Lett.* **880**, L26 (2019), arXiv:1905.02143 [astro-ph.HE].
- [18] J. Feng and Q. Wu, Constraint on the black-hole spin of M87 from the accretion-jet model, *Mon. Not. Roy. Astron. Soc.* **470**, 612 (2017), arXiv:1705.07804 [astro-ph.HE].
- [19] A. Berthureau, L. Guillemot, P. C. C. Freire, M. Kramer, V. Venkatraman Krishnan, I. Cognard, G. Theureau, M. Bailes, M. C. Bernadich, I. and M. E. Lower, Radio timing constraints on the mass of the binary pulsar PSR J1528–3146, *Astron. Astrophys.* **674**, A71 (2023), arXiv:2304.06578 [astro-ph.HE].
- [20] G. Agazie *et al.* (NANOGrav), The NANOGrav 15 yr Data Set: Observations and Timing of 68 Millisecond Pulsars, *Astrophys. J. Lett.* **951**, L9 (2023), arXiv:2306.16217 [astro-ph.HE].
- [21] V. Bozza, Quasiequatorial gravitational lensing by spinning black holes in the strong field limit, *Phys. Rev. D* **67**, 103006 (2003), arXiv:gr-qc/0210109.
- [22] V. Bozza, F. De Luca, G. Scarpetta, and M. Sereno, Analytic Kerr black hole lensing for equatorial observers in the strong deflection limit, *Phys. Rev. D* **72**, 083003 (2005), arXiv:gr-qc/0507137.
- [23] V. Bozza, F. De Luca, and G. Scarpetta, Kerr black hole lensing for generic observers in the strong deflection limit, *Phys. Rev. D* **74**, 063001 (2006), arXiv:gr-qc/0604093.
- [24] G. N. Gyulchev and S. S. Yazadjiev, Kerr-Sen dilatonic black hole lensing in the strong deflection limit, *Phys. Rev. D* **75**, 023006 (2007), arXiv:gr-qc/0611110.
- [25] M. Sereno and F. De Luca, Analytical Kerr black hole lensing in the weak deflection limit, *Phys. Rev. D* **74**, 123009 (2006), arXiv:astro-ph/0609435.
- [26] M. C. Werner and A. O. Petters, Magnification relations for Kerr lensing and testing Cosmic Censorship, *Phys. Rev. D* **76**, 064024 (2007), arXiv:0706.0132 [gr-qc].
- [27] V. Bozza and G. Scarpetta, Strong deflection limit of black hole gravitational lensing with arbitrary source distances, *Phys. Rev. D* **76**, 083008 (2007), arXiv:0705.0246 [gr-qc].
- [28] S.-W. Wei, Y.-X. Liu, C.-E. Fu, and K. Yang, Strong field limit analysis of gravitational lensing in Kerr-Taub-NUT spacetime, *JCAP* **10**, 053, arXiv:1104.0776 [hep-th].
- [29] T. Hsieh, D.-S. Lee, and C.-Y. Lin, Strong gravitational lensing by Kerr and Kerr-Newman black holes, *Phys. Rev. D* **103**, 104063 (2021), arXiv:2101.09008 [gr-qc].
- [30] K. S. Virbhadra, Relativistic images of Schwarzschild black hole lensing, *Phys. Rev. D* **79**, 083004 (2009), arXiv:0810.2109 [gr-qc].
- [31] K. S. Virbhadra and G. F. R. Ellis, Schwarzschild black hole lensing, *Phys. Rev. D* **62**, 084003 (2000),

- arXiv:astro-ph/9904193.
- [32] M. B. Jahani Poshteh and R. B. Mann, Gravitational Lensing by Black Holes in Einsteinian Cubic Gravity, *Phys. Rev. D* **99**, 024035 (2019), arXiv:1810.10657 [gr-qc].
- [33] A. Ashoorioon, M. B. Jahani Poshteh, and R. B. Mann, Distinguishing a Slowly Accelerating Black Hole by Differential Time Delays of Images, *Phys. Rev. Lett.* **129**, 031102 (2022), arXiv:2210.10762 [gr-qc].
- [34] K. Akiyama *et al.* (Event Horizon Telescope), First M87 Event Horizon Telescope Results. VI. The Shadow and Mass of the Central Black Hole, *Astrophys. J. Lett.* **875**, L6 (2019), arXiv:1906.11243 [astro-ph.GA].
- [35] G. L. Israel *et al.*, An accreting pulsar with extreme properties drives an ultraluminous x-ray source in NGC 5907, *Science* **355**, 817 (2017), arXiv:1609.07375 [astro-ph.HE].
- [36] O. Burke, J. R. Gair, J. Simón, and M. C. Edwards, Constraining the spin parameter of near-extremal black holes using LISA, *Phys. Rev. D* **102**, 124054 (2020), arXiv:2010.05932 [gr-qc].
- [37] K. S. Thorne, Disk accretion onto a black hole. 2. Evolution of the hole., *Astrophys. J.* **191**, 507 (1974).
- [38] Y. J. Guo *et al.*, PSR J2222–0137 - I. Improved physical parameters for the system, *Astron. Astrophys.* **654**, A16 (2021), arXiv:2107.09474 [astro-ph.HE].
- [39] M. Serylak *et al.*, The eccentric millisecond pulsar, PSR J0955–6150 - I. Pulse profile analysis, mass measurements, and constraints on binary evolution, *Astron. Astrophys.* **665**, A53 (2022), arXiv:2203.00607 [astro-ph.HE].
- [40] A. Corongiu *et al.*, PSR J1910–5959A: A rare gravitational laboratory for testing white dwarf models, *Astron. Astrophys.* **671**, A72 (2023), arXiv:2301.04055 [astro-ph.HE].
- [41] J. Strader *et al.*, The Densest Galaxy, *Astrophys. J. Lett.* **775**, L6 (2013), arXiv:1307.7707 [astro-ph.CO].
- [42] A. C. Seth *et al.*, A supermassive black hole in an ultra-compact dwarf galaxy, *Nature* **513**, 398 (2014), arXiv:1409.4769 [astro-ph.GA].
- [43] Y. Lian, Z. Pan, H. Zhang, P. C. C. Freire, S. Cao, and L. Qian, Discovery and Timing Analysis of New Pulsars in Globular Cluster NGC 5024: New Observations from FAST, *Astrophys. J. Lett.* **951**, L37 (2023), arXiv:2306.09741 [astro-ph.HE].